A Journey Through Expanding Cosmic Voids - How the Environment Affects Galaxy Evolution

Anita Schiller

Munich 2024

Eine Reise durch die wachsende Leere - Der Einfluss der Umgebung auf die Galaxienentwicklung

Anita Schiller

München 2024

A Journey Through Expanding Cosmic Voids - How the Environment Affects Galaxy Evolution

Anita Schiller

Bachelor's Thesis

at the University Observatory Munich

Ludwig Maximilian University

Submitted by

Anita Schiller

born in Bruck an der Leitha

Supervised by

Prof. Dr. Klaus Dolag

Dr. Rhea S. Remus

Benjamin Seidel

Munich, June 17th 2024

Contents

Chapter 1

Introduction

> "Look up at the stars and not down at your feet. Try to make sense of what you see, and wonder about what makes the universe exist. Be curious."
>
> Stephen Hawking

The large scales of the universe are seemingly mysterious and have puzzled mankind for a long time. The goal of this thesis is to shed some light on the endless darkness of the universe, finding a small piece that contributes to completing the puzzle of how the universe evolves. .

Since the beginning of the 17th century with the development of telescopes, the search for distinctively agglomerated matter in the sky was becoming increasingly detailed. The two best-known catalogues of objects in the universe are called Messier- and New General Catalogue. The focus always had been on the search for galaxies, stars and nebulae. However, at the end of the 20th century, the importance of voids in the formation of large scale structure was gaining more acknowledgment. The universe is organized in three major components forming the cosmic web. The most visible ones are filaments, connecting complexes of superclusters. Sheets are more difficult to observe since they host more galaxies with lower luminosity. However, the enormous regions that fill most of the space are called voids, as they host very little matter, they expand and are a key component in organizing the universe to form the cosmic web (Libeskind et al., 2018).
At this point, there are two questions raised:

- How are galaxies distributed throughout the universe?
- How is this distribution affected by voids?

To find an answer, an important tool in assessing the distribution of halos along the large scale structure is the halo mass function. Calculating said function was first implemented by the Press-Schechter theory (Press & Schechter, 1974) in 1974 and was then further advanced by the Excursion Set theory (Maggiore & Riotto, 2009). Later on, when the computing capacity was sufficient to run numerical simulations, mostly based on a Λ-CDM cosmology assuming a flat universe, the halo mass function was then derived from the computed data of

a simulated universe. Schuster et al. (2023) investigated void properties and also calculated the halo mass function in the Magneticum simulations for the various resolutions described in Chapter 2. This thesis too will use two differently resolved boxes and again test the concordance between them. Additionally, the halo mass function depending on the radius of voids will be evaluated. Song & Lee (2009) did calculate the halo mass functions in voids, trying to find non gaussianities in the primordial field. In this work, the hmf of halos inside $1/4$, $1/2$, $3/4$ of the void radii and inside voids in general are calculated separately, investigating the halo distribution in increasingly underdense environments with $1/4$ of the void radius being the most underdense. Furthermore, the evolution of the halo mass functions over time will be assessed, starting at redshift $z = 4.2$ corresponding to 1.489 Gyr after the Big Bang. In box2b the simulations were running up to a redshift of $z = 0.25$ representing 10.814 Gyr after the Big Bang and box3 reached a redshift of $z = 1.9$ or 3.528 Gyr.
This thesis is structured as follows: Firstly the already known findings regarding the evolution of the universe are discussed. Secondly, using Magneticum simulations, the question of how the large scale structure of the universe affects the evolution of galaxies will be explored. In this process, cosmic voids and the galaxies contained within them play a key role. With the help of the halo mass function (hmf), some insights in the evolution of galaxies on a large scale depending on the environment will be obtained

1.1 A brief history of the universe

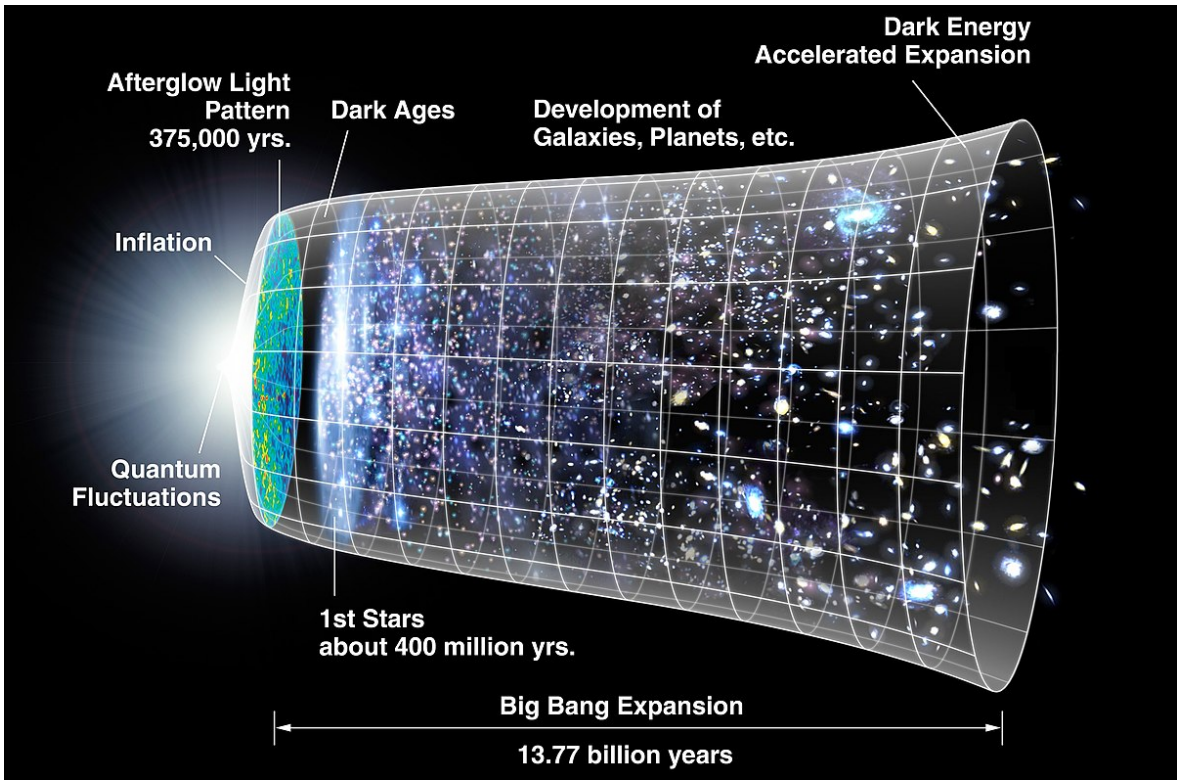

Figure 1.1: The timeline of the evolution of the universe after the Big Bang. Credits: NASA/WMAP Science Team

According to current theories, the history of the universe can be sectioned into the following chapters giving an outline of its evolution:

1.1.1 Initial cosmological singularity

For the shortest physically reasonable time period, the Planck time ($t_{PL} \approx 5.39 \cdot 10^{-44}$ seconds), the universe was in a state of infinite density and temperature.

1.1.2 Cosmic Inflation

About 10^{-36} seconds after the Big Bang the universe expanded rapidly for less than a millisecond. Whereas the Volume of the universe increased exponentially by a factor of 1078 in merely a blink of an eye. The cosmic inflation model was proposed, because it can solve some problems of the standard big bang theory, fits observational data and predicts the formation of large-scale structure quite well (Postolak, 2016).

1.1.3 Nucleogenesis and the Big Bang

After inflation ended, the energy driving the universe apart was then absorbed by matter and light. This led to what is commonly known as the Big Bang. A second later the universe was extremely hot with approximately $10^{10}\ °C$. We can not look back that far in time since all the

photons were caged in the hot "soup" because light was constantly scattered by free electrons. In this process, the first baryons (i.e. protons and neutrons) started to merge to form mainly hydrogen and helium. However, they still did not bind electrons since the temperature still did not allow them to be bound to the nuclei.

1.1.4 Cooling and Recombination

The hot universe started to cool gradually and 380,000 years after the Big Bang many electrons were bound to a nucleus, allowing for the photons to finally break free, leaving us with what we call the Cosmic Microwave Background (CMB) (Nasa, 2020).

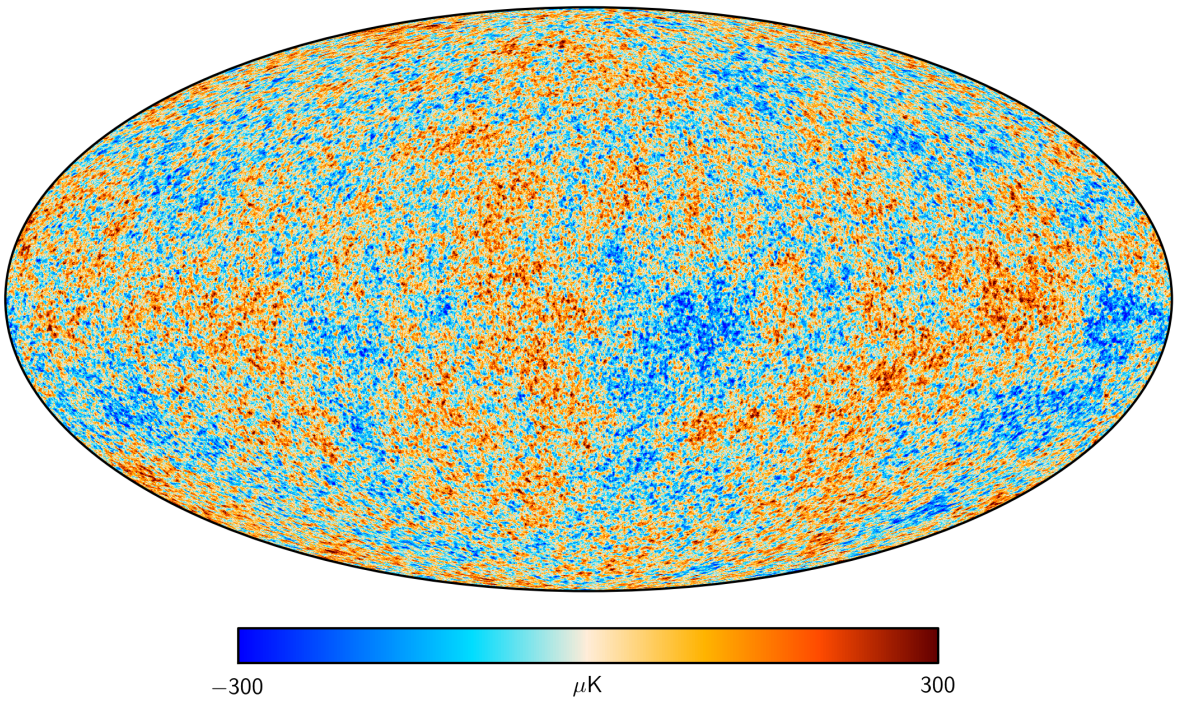

Figure 1.2: Image of the Cosmic Microwave Background made during the Planck mission. Credits: ESA and the Planck Collaboration

Since the data for the CMB was measured with very little error by Planck Collaboration et al. (2016), it provides the best constraints on the current theories of cosmology. Nearly scale-invariant Gaussian fluctuations qualify best for describing the CMB, which are also used to set up numerical simulations (see Chapter 2).

Figure 1.2 shows the temperature fluctuations of the CMB, representing the anisotropies that were rising from the initial conditions at a redshift $z \sim 1000$ (Schneider, 2008). The temperature fluctuations directly correlate with density fluctuations, again in the shape of a Gaussian field, whith the red and blue spots in Figure 1.2 representing over- and underdensities respectively. Voids will arise from those underdensities and are explicated in the following chapter.

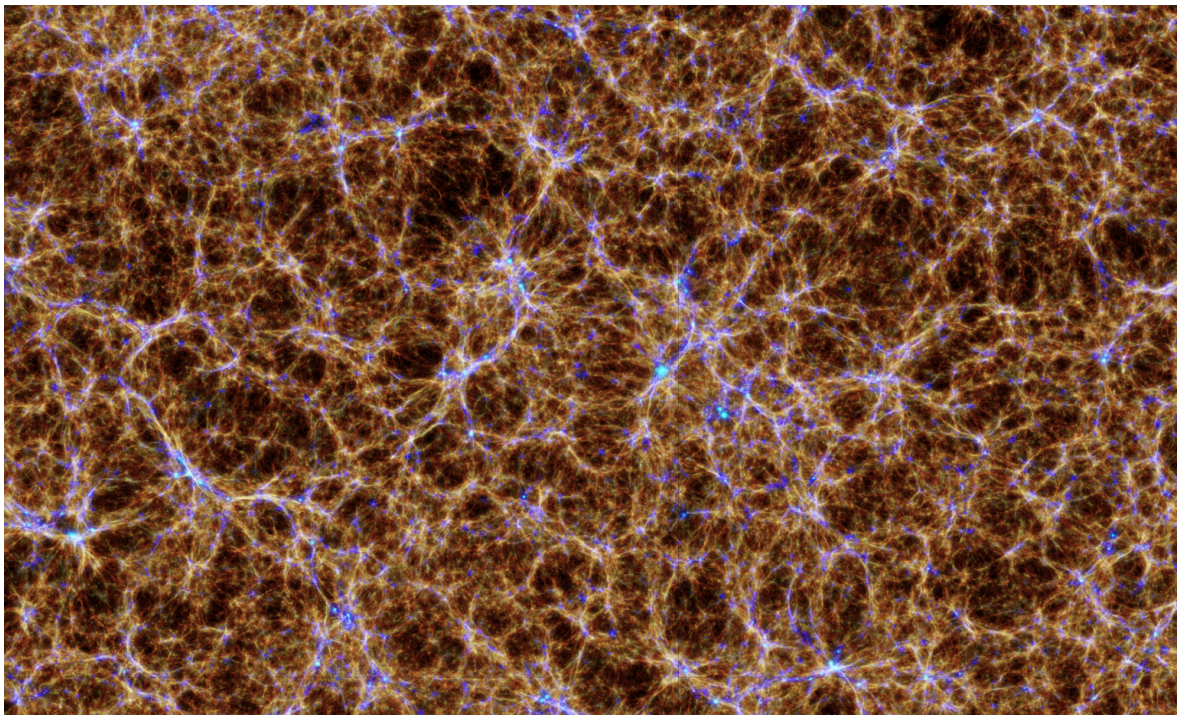

Figure 1.3: Image of the Cosmic Web. Credits: Dolag et al. (2015)

1.2 Voids

To understand what voids are, it is necessary to zoom out and picture the large scale structure of our universe. As it was found in wide-field spectroscopic galaxy surveys, galaxies form and merge in a web like structure connected by filaments that make up the Cosmic Web (Figure 1.3) (Hoosain et al., 2024). The in-between that fills the rest of the universe is composed of so-called voids (represented by the dark spots in (Figure 1.3)). As the name suggests, in opposition to the Web along which most of the mass conglomerates, voids are underdense regions. However, they make up most of the space with an estimated 95% of the total volume. The sizes of voids range from 20 to 50 Mpc h^{-1}, although the typical sizes depend on the definition of voids(Sheth & van de Weygaert, 2004). Another property of voids is that unlike galaxies, which eventually collapse and form more dense regions over time, they expand and grow until reaching their full size. Since voids are underdense regions, they respectively show less gravitational pull than the background Universe and therefore expand faster than the Hubble flow. With time, the underdense regions become less and less dense as matter evacuates through filaments and walls. In the process, the matter merges with the rest along the Cosmic Web, building ridges around the edge of the void. Notably the matter from the void center evacuates faster than from near the ridge. This also results in the void shape approaching a sphere, since the gravitational acceleration along the shortest axis of an aspherical shape is larger than on the long axis. However, it is very rare to impossible that the void shape will form into a perfect sphere since the shape is confined in the filamentary structure of the adjacent cosmic web and therefore will always have a certain ellipticity to it. Again, either the spherical modal or the ellipsoidal description of voids is just an approximation of more complex structures.

In the process of growing, adjacent voids will eventually meet, squeezing the filament between them to form a thin wall from which the matter will evacuate as described before and the two voids are bound to form a larger joined one. Another mechanism that accounts for a decrease in the number of voids is called void-in-cloud process. In this scenario, a small void is embedded in an overdense region that will eventually collapse, squeezing the void within to obliteration. These procedures are responsible for the gap in the number of over- and underdense regions. While at the outset of the universe the number of voids and halos were approximately equal, later on, the number of voids, especially the small ones, is going to decrease (Van De Weygaert & Platen, 2011).

1.3 Void galaxies

Just like our home galaxy, the Milky Way, all galaxies consist of stars, planets, gas, and dust as well as dark matter which are gravitationally bound in their own potential. However, the environment in which galaxies form has a great impact on distinctive properties. Therefore, galaxies that inhabit voids are of special interest since they provide valuable information about galaxy formation in an isolated environment.
Void galaxies differ from those that form in overdense regions along the cosmic web, in terms that they generally tend to be less massive, star forming and mostly disk galaxies. Computer simulations suggest that voids are not entirely empty, but feature a rich substructure of thin walls and filaments. This has yet to be observationally confirmed since the nearest detected void still seems to be quite void of those structures (Kreckel et al., 2014).
Other found differences that set void galaxies apart are the typically lower stellar masses and a less red colour which represents an increased specific star formation rate. Additionally, voids generally host less early-type, more gas-rich galaxies (Hoosain et al., 2024).

1.4 Λ-CDM Cosmology

Based on observations modern cosmology assumes a universe that looks the same in any direction and would not be distinguishable, if someone from another place far away would describe it. From our point of view, the large scale universe seems to be isotropic, which suggests that we either live in a particular spherical symmetric place or the whole universe is approximately homogeneous (Peebles, 1993).
Assuming the latter, one arrives at the currently used model to describe the properties of our universe that best fits observations: the Λ-CDM model. Here Λ represents the cosmological constant and at the same time dark energy while CDM abbreviates cold dark matter. Dark energy is the hypothetical explanation for the expansion of the universe, driving the universe further apart. As described in Section 1.1, in this model, our universe formed from a hot and dense singularity starting with the Big Bang. Observations of the cosmic microwave background (CMB), obtaining the Temperature field stemming from the very first visible

light that left the hot plasma after the Big Bang, discerned that the universe consists of only 5% visible baryonic matter, e.g. gas and dust, 25% dark matter along with 70% dark energy.

1.4.1 Dark Matter

The first measurement of the mass contained within the universe by Hubble in 1926 differed from the theoretically derived value. This was first called the "missing mass" problem (Peebles, 1993). Later, while measuring the rotation curves of galaxies, a discrepancy between the measured values and the theoretically derived ones, which only accounted for the visible disk, showed. A plausible explanation was that there had to be more mass surrounding the disk in a spherical shape. Since it was not to be seen, the term "dark matter" was now used to describe the seemingly missing mass that could explain the rotation curves.

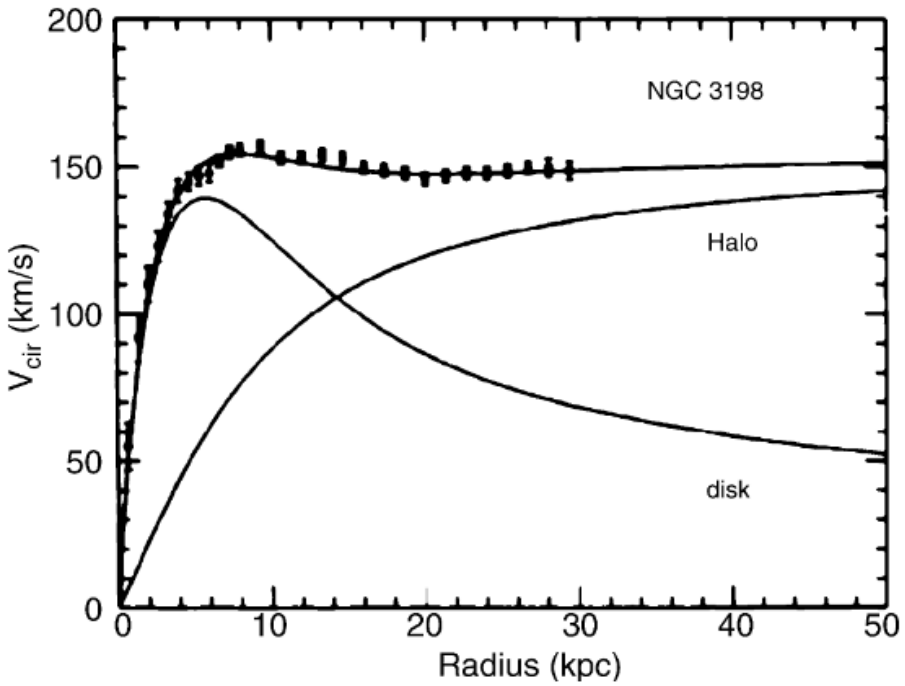

Figure 1.4: The chasm between the expected visible disk rotation curve and the measured curve of NGC 3198. This can be solved by introducing a dark matter halo. Credits: Schneider (2008)

So in short, dark matter is only interacting with baryonic matter and itself gravitationally (Schneider, 2008).

1.4.2 The expanding universe

Since the big bang the universe expands which is described by the Hubble-Lemaître parameter

$$H(t) = \frac{\dot{a}}{a} \tag{1.1}$$

where $a(t)$ represents the scale factor of the universe. In case of an expanding universe $a(t)$ also increases with time. The Hubble constant H_0 is given by the Hubble-Lemaître parameter at the present time $t = 0$(Herold, 2023). Measuring the CMB, Planck Collaboration

et al. (2016) derived the Hubble constant with a value of: $H_0 = (67.8 \pm 0.9) km\ s^{-1} Mpc^{-1}$. Today the universe is expanding with the following correlation:

$$\frac{dl}{dt} = v = H_0 \cdot l \tag{1.2}$$

where v describes the recession speed and l is the proper distance between an observer and another galaxy.
This is followed by a term for the redshift dependent on the Hubble-Lemaître parameter:

$$z = \frac{H(t) \cdot l}{c} \tag{1.3}$$

This equation makes it possible to determine the age of a galaxy at a measured redshift (Peebles, 1993).

The two notable equations describing the growth of the universe are the Friedmann equations, the derived equations of motion from the field equations of Einsteins General Relativity:

$$H^2 = \left(\frac{\dot{a}}{a}\right)^2 = \frac{8}{3}\pi G\rho_b - \frac{K}{a^2} + \frac{\Lambda}{3} \tag{1.4}$$

$$\frac{\ddot{a}}{a} = \frac{4}{3}\pi G(\rho_b + 3p) + \frac{\Lambda}{3} \tag{1.5}$$

Here, G denotes the Newtonian constant of gravity, K is the constant of integration and $\rho(t)$ as well as $p(t)$ describe the matter density and pressure respectively (Herold, 2023). The Friedmann equations give a relation of the variation of the scale factor based on the ratio of baryonic matter and dark energy.
In another step the Friedmann equations can be simplified. Considering the universe at redshift $z \lesssim 1000$ one can assume that the pressure is small compared to the mass density. Thus the Friedmann equations read:

$$H^2 = \left(\frac{\dot{a}}{a}\right)^2 = \left(\frac{\dot{z}}{1+z}\right)^2 = (H_0)^2[\Omega(1+z)^3 + \Omega_R(1+z)^2 + \Omega_\Lambda] \tag{1.6}$$

$$\frac{\ddot{a}}{a} = {H_0}^2[\Omega_\Lambda - \Omega(1+z)^3/2] \tag{1.7}$$

Ω, Ω_R and Ω_Λ are constants where $\Omega = \frac{8\pi G\rho_0}{3{H_0}^2}$ is the density parameter with ρ_0 being the present mean mass density. $\Omega_R = \frac{1}{(a_o H_0 R)^2}$ describes the curvature that is positive if R is real and therefore denotes an open universe and negative if R is imaginary, describing a closed universe. The universe we live in is considered to be flat. $\Omega_\Lambda = \frac{\Lambda}{3{H_0}^2}$ is associated with dark energy.

Chapter 2

Simulations

2.1 Magneticum

How can humans study the evolution of galaxies on large cosmic scales, when the lifespan is a mere blink of an eye compared to the billion years it takes for galaxies to evolve? Therefore, numerical simulations provide a beneficial tool, allowing to visualize the whole evolution of the universe or even to simulate what is yet to come in the future. Magneticum Pathfinder (Dolag et al., 2015) provides various numerical simulations using a flat Λ-CDM cosmology, as mentioned in Section 1.4. They are based on GADGET-3, a parallel TreeSPH code built on GADGET-2 (Springel, 2005). (SPH abbreviates "smoothed particle hydrodynamics".)

Magneticum applies a Λ-CDM cosmology with the following parameters:

- $\Omega_0 = 0.272$ (total matter density)
- $\Omega_b = 0.0456$ (baryon density)
- $\Lambda_0 = 0.728$ (cosmological constant)
- $H_0 = 70.4 kms^{-1} Mpc$ (Hubble constant)
- $n = 0.963$ (index of the primordial power spectrum)
- $\sigma_8 = 0.809$ (overall normalization of the power spectrum)

This was established based on the WMAP7 (seven-year wilkinson microwave anisotropy probe) observations by Komatsu et al. (2011). The data has been obtained from measurements of the temperature and polarization anisotropies of the CMB.

The magneticum simulations have periodic boundary conditions and provide six boxes with different sizes as shown in Figure 2.1 below (Bocquet et al., 2016).

	Box0	Box1a	Box2b	Box2	Box3	Box4	Box5
[Mpc/h]	2688	896	640	352	128	48	18
mr	$2*4536^3$	$2*1512^3$		$2*594^3$	$2*216^3$	$2*81^3$	
hr			$2*2880^3$	$2*1584^3$	$2*576^3$	$2*216^3$	$2*81^3$
uhr					$2*1536^3$	$2*576^3$	$2*216^3$
xhr						$2*1536^3$	$2*576^3$

Figure 2.1: Various box sizes in Magneticum simulations. The first line denotes the length of the edge of the box. The following lines show the resolutions (mid, high, ultra high and extra high) and the number of particles used. Credit: Dolag et al. (2015)

This thesis is based on simulations of the universe contained in a cubic box with an edge length of 640 Mpc h^{-1} for box2b and 128 Mpc h^{-1} for box3. The first box contains dark matter (dm) particles with masses of $6.9 \cdot 10^8 M_\odot h^{-1}$ and gas particles with $1.4 \cdot 10^8 M_\odot h^{-1}$. The latter consists of particles with masses $m_{dm} = 3.6 \cdot 10^7 M_\odot h^{-1}$ and $m_{gas} = 7.3 \cdot 10^6 M_\odot h^{-1}$. Therefore box3 provides a higher resolution allowing for smaller halos to be resolved while box2b has a larger sample size (Dolag et al., 2015).

Chapter 3

A statistical evaluation of the halo distribution

3.1 Methodology

The first step was to identify the voids in the box. This was done by using the Void IDentification and Examination toolkit VIDE (Sutter et al., 2014). Essentially, VIDE creates a Voronoi tessellation of the tracer particles selected from the initial particles in the box. Within one Voronoi cell, the density ρ is smoothed by assuming a constant density throughout the cell, with the volume of the corresponding Voronoi cell being proportional to $\frac{1}{\rho}$. Later on, adjacent cells are categorized into zones that are then merged together so that the conglomerated zones form a void according to Sutter et al. (2014): Adjacent zones are only added to a void if the density of the wall between them is less than 0.2 times the mean particle density.
Secondly, the halos must be identified from the particles in the boxes. Therefore, using SUBFIND (Springel et al., 2001) which identifies virialized particle groups using the friends-of-friends (FOF) algorithm, a halo catalog was retrieved from the simulations. The groups are formed by linking particles less than a specific length b away from each other. This length is chosen so that groups that are enclosed by a density of $\rho \propto 1/b^3$ are close to the virial overdensity, derived from the spherical collapse model.

The halo catalogue provided by SUBFIND was then reduced using a mass cut of $5 \cdot 10^{10} M_\odot h^{-1}$ for box2b and $5 \cdot 10^9 M_\odot h^{-1}$ for box3. This selects only halos that have a physically reasonable mass corresponding to the resolution of the box.

3.2 Halo mass function

The central part of this thesis revolves around the halo mass function (hmf) $\frac{dn}{dM}$:

$$\frac{dn(M)}{dM} = f(\sigma)\frac{\bar{\rho}}{M^2}\frac{dln\sigma^{-1}(M)}{dlnM} \tag{3.1}$$

This is the theoretically derived formula from the excursion set formalism, the extension of the Press-Schechter theory (Press & Schechter, 1974). Here n(M) is the number density of dark matter halos with mass M, $\bar{\rho}$ describes the mean density of the universe and σ^2 is the variance of the linear density field. In Press-Schechter theory $f(\sigma)$ is given by:

$$f_{PS}(\sigma) = \left(\frac{2}{\pi}\right)^{\frac{1}{2}} \frac{\delta_c}{\sigma} e^{-{\delta_c}^2/(2\sigma^2)} \tag{3.2}$$

With the assumption of a spherical collapse, $\delta_c \simeq 1.686$ represents the critical value for the collapse at redshift $z = 0$. This can be generalized for arbitrary redshifts with $\delta_c(z) = \delta_c(z = 0)/D(z)$, hereby $D(z)$ denotes the linear growth factor. According to Maggiore & Riotto (2009) the Press-Schechter formalism predicts too many low-mass halos and at the same time too few high-mass halos. This occurs since the spherical approximation is not sufficient to describe more realistic N-body simulations in which the halo formation process is of a more complex nature.
Generally, $\delta(x) = \frac{\rho(x)-\bar{\rho}}{\bar{\rho}}$ describes the density contrast dependent on the mean density $\bar{\rho}$ of the universe and x the comoving position. An object counts as virialized if $\delta(x)$ exceeds δ_c assuming a spherical collapse (Maggiore & Riotto, 2009).

The following figure shows the previously discussed density contrast on a logarithmic scale depending on the distance from a void halo. This is to visualize that overdensities actually do exist inside underdensities and not only along the cosmic web. Here $r_{tohalo} = 0$ describes the halo itself and from thereon the distance to the halo. The two halos shown are two samples of halos existing in voids, extracted from box2b. The blue line shows a void with radius $r_{Void} = 23.26$ Mpc h^{-1} and the contained halo is 4.98 Mpc h^{-1} away from the center of the void assuming a spherical shape. Another void is depicted by the orange line with a radius of $r_{Void} = 12.38$ Mpc h^{-1}. The contained halo only has an offset of 0.89 Mpc h^{-1} from the void center.
The trend of the curve from left to right with increasing distance from the halos shows the overdensity within the halo, which then drops below zero, indicating that the halo sits inside a void. When the wall of the void is reached the density contrast again increases now including a filament of the cosmic web.
Another point of interest is pictured by the dashed lines representing the void radius. It comes to mind, that those lines do not quite overlap with the increase of $\delta(x)$ along the edges of the voids.
This has two reasons:

- The halos are not located in the center of the void. So naturally, when measuring $\delta(x)$ in spheres centered around the halo position, the increase in density contrast is not aligned with the walls of the void. This is far more visible with the blue line because of the greater offset.
- The voids themselves are not perfectly spherical as discussed in Section 1.2

This should accentuate Figure 1.3 in a deepened physical sense. ....

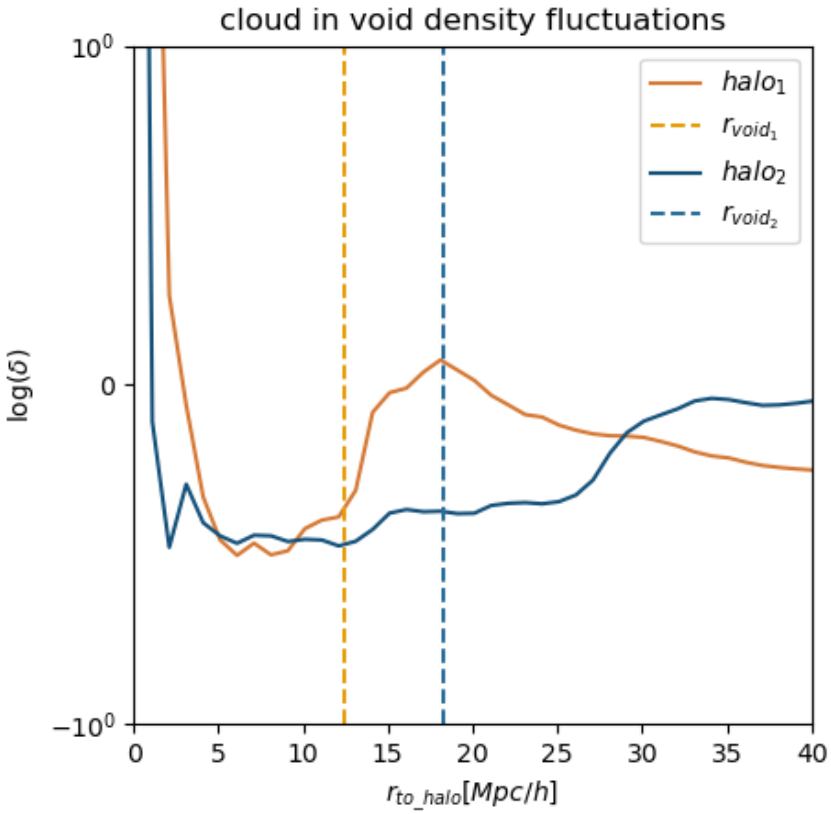

Figure 3.1: The density contrast depending on the distance from a halo inside a void.

3.2.1 The halo mass function in simulations

To create the hmf from magneticum simulations every halo in the box is matched to the closest void. Later, the halos are selected based on their position in accordance to the nearest void. For example, in order to calculate the hmf for $1/4$ of the void radius, only halos that lie within $1/4$ of their paired void are considered. For the other radii this is done accordingly. In the next step the cumulative relative frequencies N of the logarithmic mass values (plotted on the x-axis in Figure 3.2) are calculated. Here N is relative to the total count n_{all} of halos inside the given void radius, which represents the normalization. So $N = \frac{n_{step}}{n_{all}}$ where n_{step} are the counted halos within a mass range counting the halos that are added when considering a higher fraction of mass $dlog(M)$. This is performed by counting all halos showing a mass smaller than the respective mass value and dividing them by the total number of halos in box2b. Lastly the derivative $\frac{dN}{dlog(M_{halo})}$ results in the halo mass function.

Beginning with the halo mass functions at redshift $z = 0.25$ for various void radii shown in Figure 3.2, the first apparent effect is the splitting of the hmf. This occurs because matter agglomerates along the cosmic web, allowing for bigger, partly merged halos outside of voids. Since matter evacuates the void from within (see Section 1.2), there is yet more mass available in the outer parts of the void than deep within. So, the higher fraction of the void radius that is considered, the bigger the halos can get, within that range.

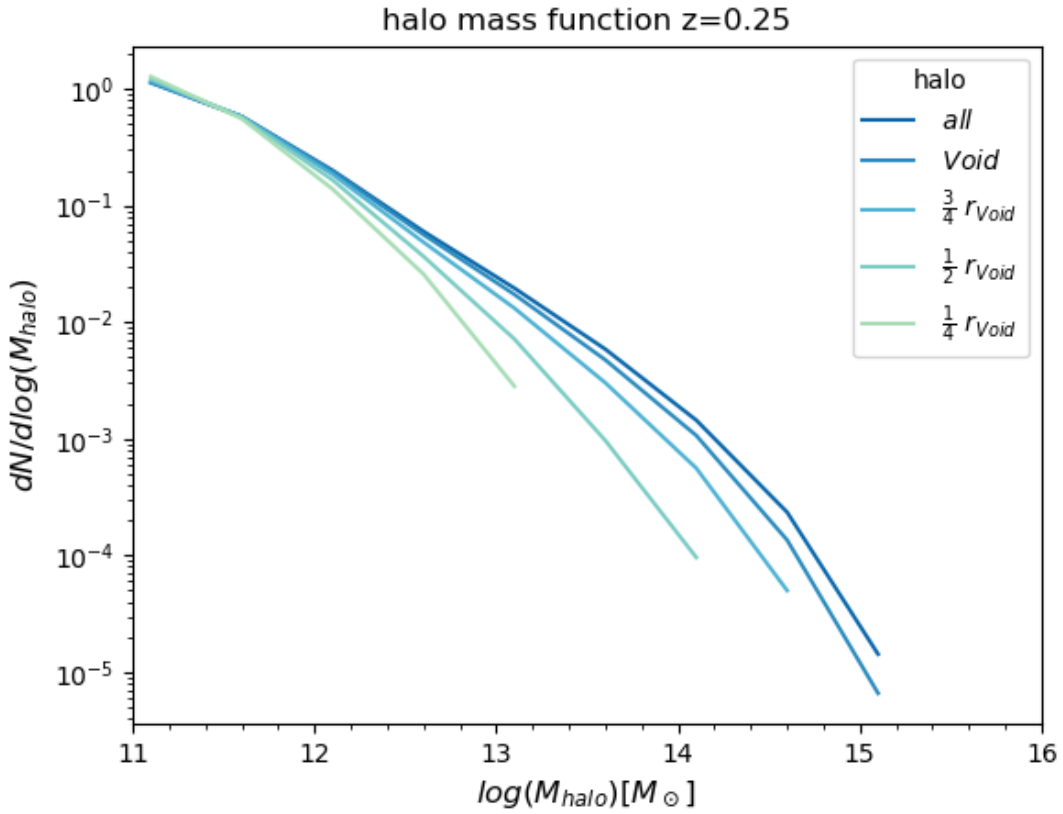

Figure 3.2: Halo mass function depending on the position in voids at redshift $z = 0.25$ in box2b. The leftmost light-colored branch includes all halos that sit within one fourth of the void radius. From there on, the branches to the right of the light one increase the radius until all halos inside voids are considered. Lastly, the darkest, longest branch evaluates all halos inside the box.

A thought experiment might offer some insight here:
Imagine a lake, glinting in a light turquoise color reflecting trees that surround it. Visualizing diving into the lake, the deeper one descends the darker the color of the lake gets, being a rich dark blue at the bottom.
Suppose a galaxy sits on top of a lake, surrounded by air, while being able to accrete and merge with water, it is intuitive, that the galaxy on top of the lake has little material available to grow bigger. However, if the galaxy were to dive just a bit deeper into the lake, it would then wholly covered by water. Now more fluid surrounds it, although it still weighs lightly on the galaxy since the pressure of the water above is minimal near the surface. On the other hand, if the galaxy were to be at the bottom of the lake, even more water would weigh down on it making it easier to merge with the surrounding water, thus at the bottom of the lake one would find the largest galaxies.
Here the depth of the lake represents the gravitational pull at a point in the universe and at the same time the relative mass density $\delta(x)$ (the deeper the lake, the higher $\delta(x)$).

The colors in Figure 3.2 show exactly that. the lightest color represents halos inside $1/4$ of the void radius where not a lot of matter is available this deep inside the void, hence only halos containing a small mass show up. The further one approaches the cosmic web where

most halos are agglomerated, matter is more accessible, and therefore higher mass halos are able to form.

3.2.2 A journey through time

At this point, the question of how the halo mass function evolves with time occurs. So a step back in time means evaluating an earlier snapshot from the Magneticum simulations, now considering redshift $z = 1.9$ in box2b.

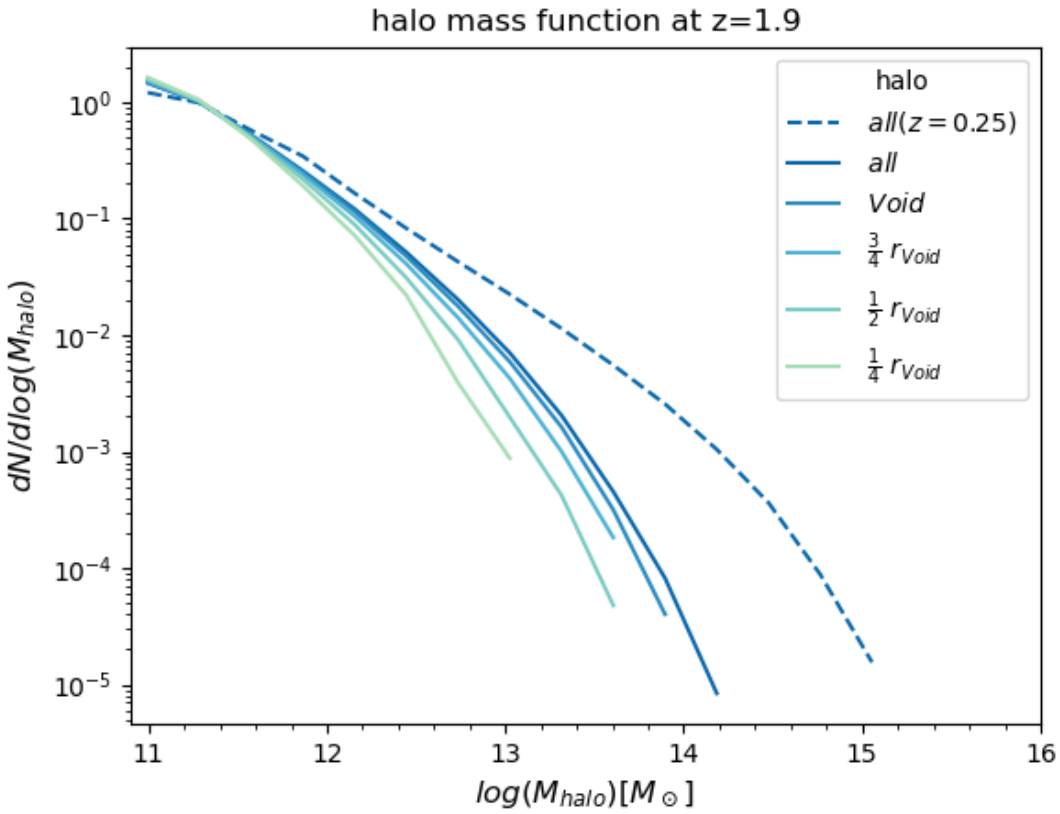

Figure 3.3: Halo mass function at z = 1.9 depending on the position in voids in box2b. Analogous to Figure 3.2 the colors represent halos from the smallest fraction of the void radius to all halos, in light to dark colors respectively. The dark blue dashed line depicts the hmf calculated with all halos at redshift $z = 0.25$

Studying the evolution of the hmf, again in box2b, over time an interesting aspect is, that there is a difference between the darkest blue line, picturing all halos at z = 1.9 and the dashed line, representing the hmf of all halos from the previous plot, Figure 3.2 at z = 0.25. At this point, it is useful to establish a general timetable, which structure formation follows. However, this presents only a rough estimate developed in 1991 and is to be considered as such.

notable structure	time
Gravitational potential fluctuations	$z \gtrsim 10^3$
Spheroids of galaxies	$z \sim 20$
The first engines for active galactic nuclei	$z \gtrsim 10$
The intergalactic medium	$z \sim 10$
Dark matter	$z \gtrsim 5$
Dark halos of galaxies	$z \sim 5$
Angular momentum of rotation of galaxies	$z \sim 5$
The first 10 % of heavy elements	$z \gtrsim 3$
Cosmic magnetic fields	$z \gtrsim 3$
Rich clusters of galaxies	$z \sim 2$
Thin disks of spiral galaxies	$z \sim 1$
Superclusters, walls and voids	$z \sim 1$

Table 3.1: A rough timeline of structure formation.

Especially the last entry raises questions since in the simulations we can find voids well back to redshifts of ~ 7. Depicted in Figure 3.4 are the many voids with their respective radii at a redshift of $z = 6.9$ found in the Magneticum simulations using VIDE (Sutter et al., 2014).

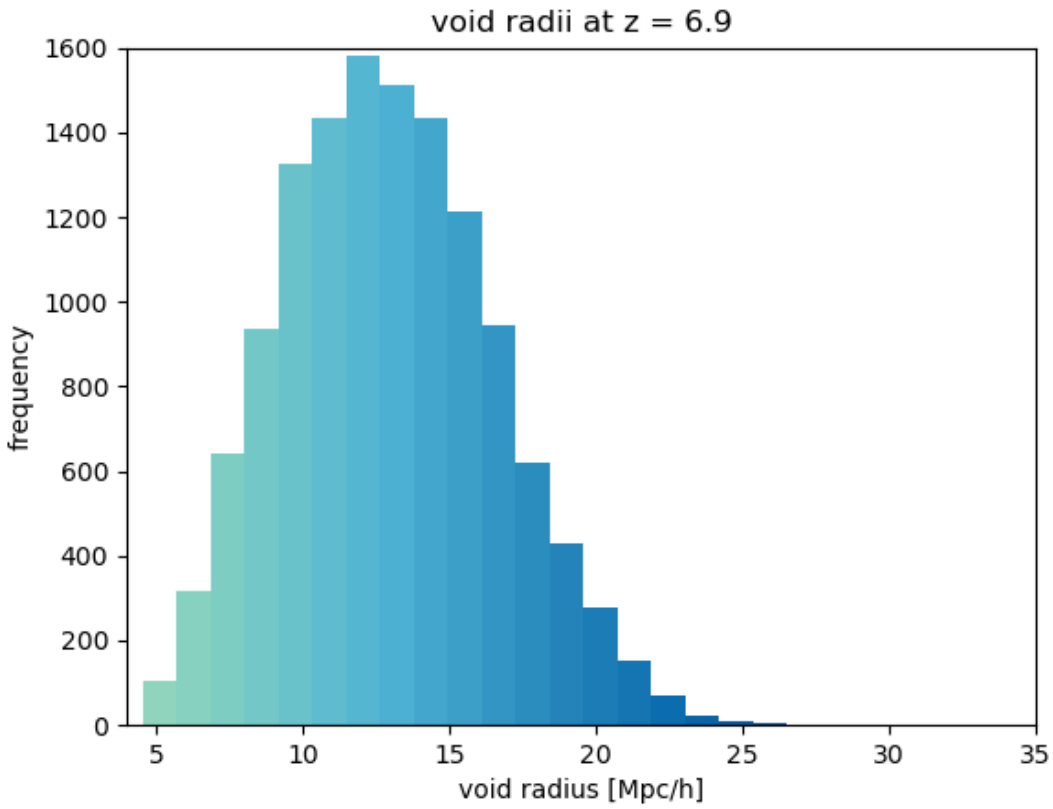

Figure 3.4: Histogram of the found void radii in box2b at redshift $z = 6.9$

According to Peebles (1993) this categorization is justified by the following: "The voids and sheets have been assigned an assembly redshift somewhat less than that of the rich clusters, because they look like less dense and less well advanced parts of the same hierarchical clustering phenomenon" (p. 613). Again this argument has to be seen in relation to the scientific

knowledge of the time. However, the formation of dark halos seems to be more accurate since statistically the halo mass function could be established from a redshift of $z \leqslant 4.2$ as shown in Figure 3.5.

Circling back to the initially discussed halo mass function in Figure 3.3. The question of why the dark blue line differs from the dashed dark blue line can be answered by the simple fact that halos accrete nearby mass and can merge with time. Hence it follows, that the halo mass function of all halos at redshift $z = 0.25$ shows halos containing higher masses than at redshift $z = 1.9$
Another characteristic feature of the hmf at $z = 1.9$ is the less significant split up between the halo mass functions considering halo positioning inside voids. This can be explained by the same principle. However, it is easier to picture the split up with increasing time, going from redshift $z = 1.9$ to $z = 0.25$. The outflow of matter from inside the void amounts to a less dense interior and an increasing amount of matter in the outskirts. Therefore, not only the hmf considering all voids flattens out and becomes less steep, but the halos contained in voids follow the same principle. However, the intensity of the flattening decreases the further inside a void one dares to look.

Taking this a step further back in time, one finds Figure 3.5:

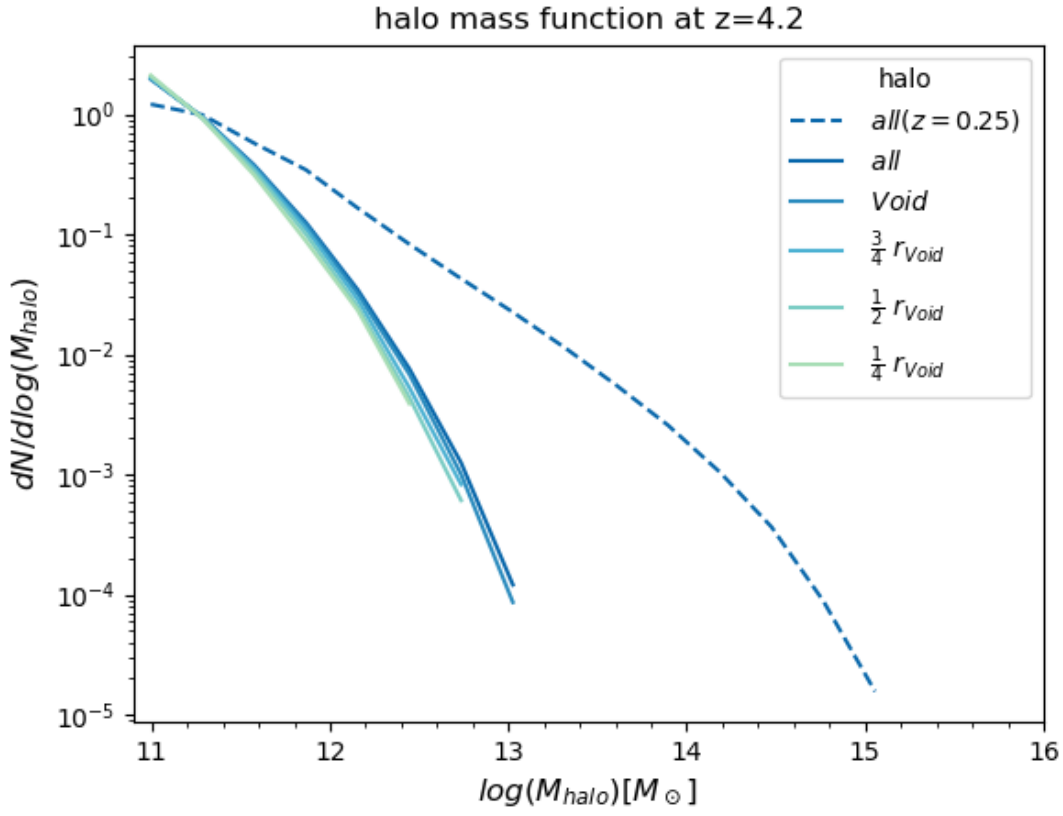

Figure 3.5: Halo mass function at z = 4.2 depending on the position in voids. The colors represent the same as in the figures before.

The splitting between the different void radii is now rather insignificant. Since at time $z = 4.2$ only small halos populate the universe, they are more equally distributed throughout the whole box. The big halos are going to develop from there on, mostly in overdense regions, while the halos inside the voids stay rather small.

3.2.3 Entering another box

While the observations in the last chapter were all derived from box2b, the halo mass function will now also be calculated for box3. This provides a sanity check of the previous findings and also has the advantage of being able to obtain a higher resolution as described in Chapter 2.

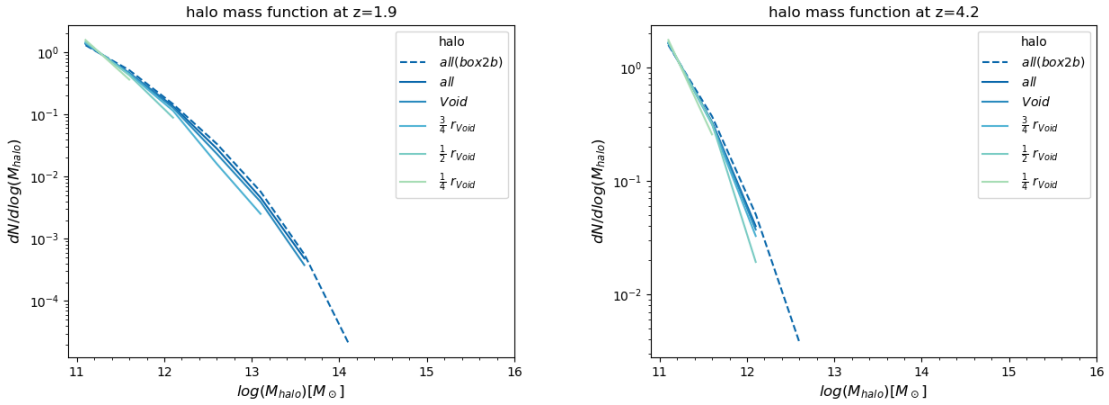

Figure 3.6: Halo mass functions obtained from box3 at various redshifts with the same mass cut for both boxes.

Using the same mass cut for both boxes one obtains a converging curve, that shows the agreement between the two boxes. However, then the advantage of box3, being able to resolve smaller halos, is neglected.

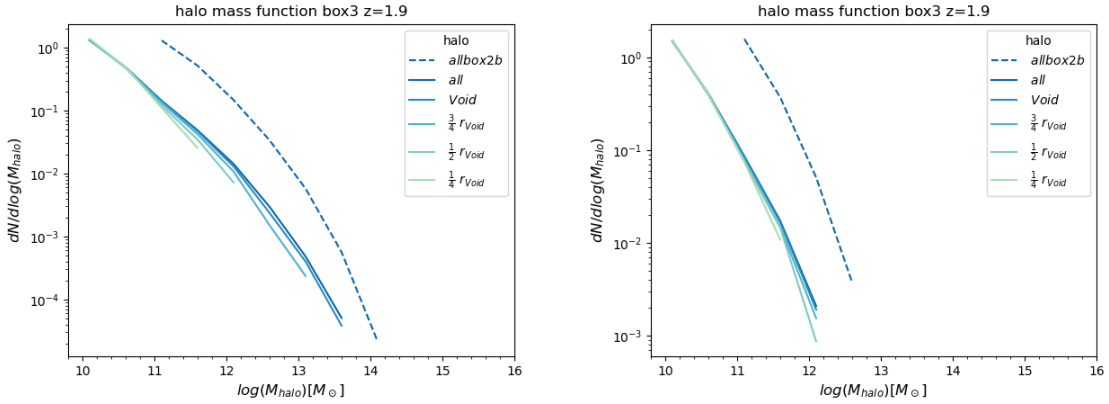

Figure 3.7: Halo mass functions obtained from box3 at various redshifts with a smaller mass cut for box3.

Including the smaller mass cut, the halo mass functions differ between the boxes as shown in Figure 3.7. This is due to the fact, that the previously used normalization can not be

applied here if the values should be comparable. Before, the halo count was normalized with respect to the overall count within the span of the smallest, least massive halo to the biggest one found in the box or inside any radius of voids. As discussed before, there are higher mass halos traceable outside of voids, consequently, the drop in the curve occurs earlier for the hmf inside voids (and even prior to that, the further inside of voids the hmf is calculated). This occurrence pictures the physical explanation but is also implemented in the norm. If one were to normalize all the curves with respect to the same range from the overall smallest to the generally biggest halo, the curves would show a similar trend as in Figure 3.7

In short, the first used norm was applicable for box2b as well as box3 since the used mass ranges were the same and therefore calculated the relative cumulative frequency regarding the same range minus the cut-off at the high mass end. However, if the smaller masses resolved by box3 are incorporated, the normalization needs to be adjusted in order to achieve comparable halo mass functions.

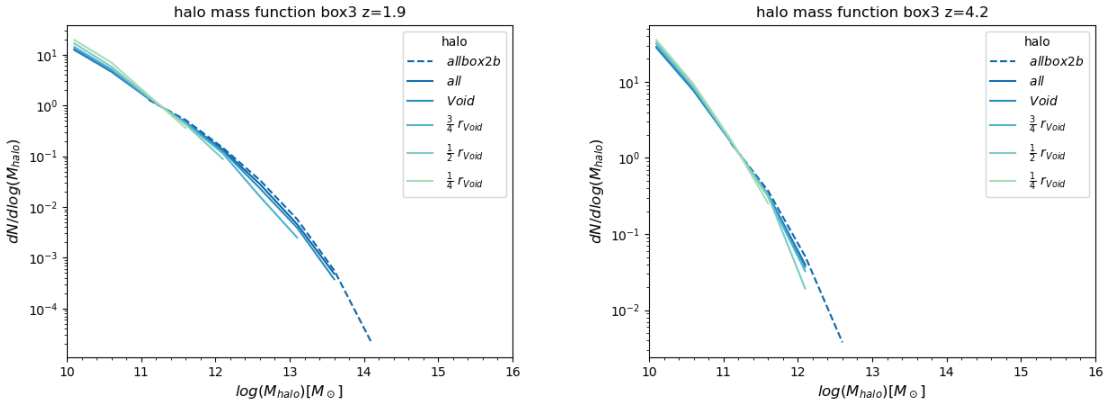

Figure 3.8: Halo mass functions obtained from box3 at various redshifts with a smaller mass cut for box3 and a unified norm.

To achieve a comparable result, the normalization has to be in accordance to the mass range from the smallest halo contained in box2b to the respective largest halo. Now the results shown in Figure 3.8 agree in the range pictured in Figure 3.6, the low mass end, however, shows a shift compared to the low mass end in Figure 3.7. It catches the eye, that here the low mass end deviates further from another than in Figure 3.7. Notably, the curve depicting halos within one fourth of the void radius is shifted upward the most. This is due to the fact that, the normalization factor is the smallest in this case since the range of the masses of the halos contained this deep inside voids has the least cross section with the range of box2b. At the same time, inside voids the relative frequency of small halos is the highest, therefore, the absolute value of small halos over said normalization is the highest, resulting in the highest starting point of the hmf. This effect is less prominent for the hmf within 1/2 of the void radius since the overlap with the mass range of box2b is now higher, resulting in a greater total frequency which is used as normalization. Therefore, the hmf of $1/2r_{void}$ is shifted

downward compared to the hmf of $1/4r_{void}$ and so on.

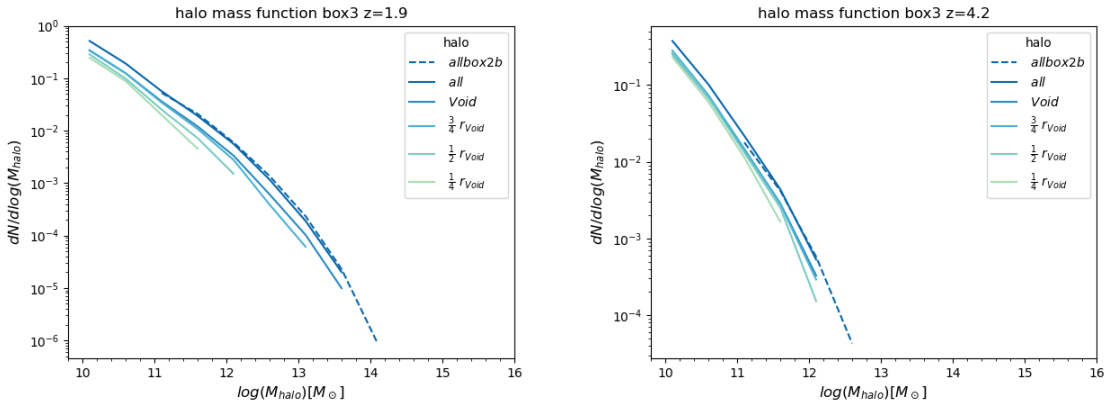

Figure 3.9: Halo mass functions obtained from box3 at various redshifts with a smaller mass cut for box3 and a unified norm.

The previous findings can be further advanced when introducing a volume normalization. Now the values are not divided by the overall count within a given mass range, but rather the Volume enclosed. Again, the curves from both boxes align. However, the shifting of the halo mass functions as described previously, is now reversed. The hmf regarding $1/4r_{void}$ is now shifted to the lowest point on the y-axis, due to the fact that voids are most underdense on the inside. Therefore, the halos counted with respect to the volume enclosed by $1/4r_{void}$ are relatively least frequent. On the other hand, the hmf considering halos inside the whole box shows the highest y-value since here the overdense cosmic web is enclosed. So, this normalization also provides information regarding the density within the sampled volume.

The one thing staying constant across all the presented normalizations is the gradient of the halo mass functions which holds the most valuable information. That being the relative added amount of halos per step. The steeper the curve, the less halos are added containing more mass than the ones in the previous step. So, it indicates the distribution of the halos throughout the different mass ranges.

Chapter 4

Conclusion

Following this journey through time, from the beginning of the universe to the evolution of voids and the galaxies inhabiting them, some insights could be obtained. With the help of Magneticum simulations and important observational evidence, measuring the CMB in order to match the cosmological parameters, it is possible to create a whole universe inside a box. Studying this evolution, with the halo mass function as the main tool, we obtained the following:

The matter distribution and thereby the halo distribution in the universe follows an interesting pattern. Generally, halos form everywhere throughout the entire box but there are certain massive halos that can only be found in a dense environment. While matter starts to agglomerate and collapse, cosmic voids are growing, hence providing an environment for smaller halos or rather prohibiting large halos from forming. This is caused by the absence of matter driven by the outflowing motion gradually emptying voids. How can something grow when there is nothing to accumulate?

In the beginning, halos start to form everywhere throughout the box. However, at $z = 4.2$ the differences in the distribution start to show. While the small halos still form everywhere, bigger halos tend to live outside of voids. This is beautifully depicted by the evolution of the halo mass function. The further it evolves in time, the bigger halos can be found. That is displayed by the splitting of the halo mass function, which at the same time is reflected by the normalization. While the halos deep inside voids stay rather small, the more dense the environment gets, the bigger halos can be found. This would point to a slowed galaxy evolution inside voids, which could be of great use for detailed studies of galaxy evolution and star formation. It is also interesting to see that the slowed galaxy growth is dependent on the position inside the void. The further inside a void the halos are positioned, the less massive they are. So, one could argue that the evolution of galaxies does depend on the environment, and in that sense, voids play an important role since they represent underdense regions with the void center being the most devoid of matter.

The fact that those findings are consistent between the two boxes shows that systematic errors regarding different resolutions can be ruled out. However, there are constraints to this approach since the used box needs to have a sufficient resolution but at the same time has to be big enough to host a statistically significant halo and void catalog. Another point to keep in mind is the definition of voids that is given by VIDE (Sutter et al., 2014), being able to find more accurate void shapes than assumed in theoretical spherical models. However, at the same time, the found voids at a redshift of $z = 0.25$ only make up about 50% of the box volume if one estimates the volume based on spherical voids with an effective radius as done in this thesis.
Still, this does not negate the previously discussed findings since it might only shift the halo mass function inside voids closer to the hmf considering all halos inside the box regardless of their position. The same effect, a slightly less steep function, would show for all halo mass functions inside voids since the fractions of their radius would also scale accordingly when the void would actually be bigger. This is due to the fact that if the void size would be underestimated now, then some bigger halos that now lie outside voids might actually be inside a void radius but regardless, the overall findings should remain unchanged.

Building upon this work, it could be of interest to incorporate the ellipticity of voids ensuring a more accurate tracing of the halo environment instead of the spherical approach. It also would be expected that the halo mass functions would freeze at some point in the future at a higher redshift. That is because at some point voids will stop growing and galaxies will be too far apart to merge any further, if the universe were to still expand, driven by a Λ dominated universe. This can already be seen in the splitting of the hmf since the one including halos within one fourth of the void radius is changing slower than the others. Hence, the halo mass function is a very useful tool in assessing halo evolution in different environments and can be used for future evaluations.

References

Bocquet, S., Saro, A., Dolag, K., & Mohr, J. J. (2016). Halo mass function: Baryon impact, fitting formulae and implications for cluster cosmology. *Monthly Notices of the Royal Astronomical Society*, *456*(3), 2361–2373. ArXiv:1502.07357 [astro-ph].
URL http://arxiv.org/abs/1502.07357

Dolag, et al. (2015). Magneticum. Last accessed 14.Juli 2024.
URL http://www.magneticum.org/media.html

Herold, L. (2023). *Resolving the Hubble Tension with Early Dark Energy*. Doctoral dissertation, Ludwig–Maximilians–Universität München.

Hoosain, M., Blyth, S.-L., Skelton, R. E., Kannappan, S. J., Stark, D. V., Eckert, K. D., Hutchens, Z. L., Carr, D. S., & Kraljic, K. (2024). The effect of cosmic web filaments on galaxy properties in the RESOLVE and ECO surveys. ArXiv:2401.09114 [astro-ph].
URL http://arxiv.org/abs/2401.09114

Komatsu, E., Smith, K. M., Dunkley, J., Bennett, C. L., Gold, B., Hinshaw, G., Jarosik, N., Larson, D., Nolta, M. R., Page, L., Spergel, D. N., Halpern, M., Hill, R. S., Kogut, A., Limon, M., Meyer, S. S., Odegard, N., Tucker, G. S., Weiland, J. L., Wollack, E., & Wright, E. L. (2011). SEVEN-YEAR *WILKINSON MICROWAVE ANISOTROPY PROBE* (*WMAP*) OBSERVATIONS: COSMOLOGICAL INTERPRETATION. *The Astrophysical Journal Supplement Series*, *192*(2), 18.
URL https://iopscience.iop.org/article/10.1088/0067-0049/192/2/18

Kreckel, K., Van Gorkom, J. H., Beygu, B., Van De Weygaert, R., Van Der Hulst, J. M., Aragon-Calvo, M. A., & Peletier, R. F. (2014). The Void Galaxy Survey: Galaxy Evolution and Gas Accretion in Voids. *Proceedings of the International Astronomical Union*, *11*(S308), 591–599.
URL https://www.cambridge.org/core/product/identifier/S1743921316010644/type/journal_article

Libeskind, N. I., Van De Weygaert, R., Cautun, M., Falck, B., Tempel, E., Abel, T., Alpaslan, M., Aragón-Calvo, M. A., Forero-Romero, J. E., Gonzalez, R., Gottlöber, S., Hahn, O., Hellwing, W. A., Hoffman, Y., Jones, B. J. T., Kitaura, F., Knebe, A., Manti, S., Neyrinck, M., Nuza, S. E., Padilla, N., Platen, E., Ramachandra, N., Robotham, A., Saar, E., Shandarin, S., Steinmetz, M., Stoica, R. S., Sousbie, T., & Yepes, G. (2018). Tracing

the cosmic web. *Monthly Notices of the Royal Astronomical Society*, *473*(1), 1195–1217.
URL http://academic.oup.com/mnras/article/473/1/1195/4062204

Maggiore, M., & Riotto, A. (2009). The Halo Mass Function from Excursion Set Theory. I. Gaussian fluctuations with non-markovian dependence on the smoothing scale. ArXiv:0903.1249 [astro-ph, physics:gr-qc, physics:hep-ph, physics:hep-th].
URL http://arxiv.org/abs/0903.1249

Nasa (2020). Cosmic history. Last accessed 5.Juni 2024.
URL https://science.nasa.gov/universe/overview/

Peebles, P. (1993). *Principles of Physical Cosmology*. Princeton University Press.

Planck Collaboration, Ade, P. A. R., & Aghanim, e. a. (2016). Planck 2015 results. XIII. Cosmological parameters. *Astronomy & Astrophysics*, *594*, A13. ArXiv:1502.01589 [astro-ph].
URL http://arxiv.org/abs/1502.01589

Postolak, M. (2016). Did the Big Bang and cosmic inflation really happen? (A tale of alternative cosmological models).

Press, W. H., & Schechter, P. (1974). Formation of Galaxies and Clusters of Galaxies by Self-Similar Gravitational Condensation. *The Astrophysical Journal*, *187*, 425.
URL http://adsabs.harvard.edu/doi/10.1086/152650

Schneider, P. (2008). *Einführung in die Extragalaktische Astronomie und Kosmologie*. Springer-Verlag Berlin Heidelberg.

Schuster, N., Hamaus, N., Dolag, K., & Weller, J. (2023). Why Cosmic Voids Matter: Nonlinear Structure & Linear Dynamics. *Journal of Cosmology and Astroparticle Physics*, *2023*(05), 031. ArXiv:2210.02457 [astro-ph].
URL http://arxiv.org/abs/2210.02457

Sheth, R. K., & van de Weygaert, R. (2004). A hierarchy of voids: Much ado about nothing. *Monthly Notices of the Royal Astronomical Society*, *350*(2), 517–538. ArXiv:astro-ph/0311260.
URL http://arxiv.org/abs/astro-ph/0311260

Song, H., & Lee, J. (2009). THE MASS FUNCTION OF VOID GROUPS AS A PROBE OF PRIMORDIAL NON-GAUSSIANITY. *The Astrophysical Journal*, *701*(1), L25. Publisher: The American Astronomical Society.
URL https://dx.doi.org/10.1088/0004-637X/701/1/L25

Springel, V. (2005). The cosmological simulation code GADGET-2. *Monthly Notices of the Royal Astronomical Society*, *364*, 1105–1134. Publisher: OUP ADS Bibcode: 2005MNRAS.364.1105S.
URL https://ui.adsabs.harvard.edu/abs/2005MNRAS.364.1105S

Springel, V., White, S. D. M., Tormen, G., & Kauffmann, G. (2001). Populating a cluster of galaxies – I. Results at z ¼ 0.

Sutter, P. M., Lavaux, G., Hamaus, N., Pisani, A., Wandelt, B. D., Warren, M. S., Villaescusa-Navarro, F., Zivick, P., Mao, Q., & Thompson, B. B. (2014). VIDE: The Void IDentification and Examination toolkit. ArXiv:1406.1191 [astro-ph].
URL http://arxiv.org/abs/1406.1191

Van De Weygaert, R., & Platen, E. (2011). COSMIC VOIDS: STRUCTURE, DYNAMICS AND GALAXIES. *International Journal of Modern Physics: Conference Series*, *01*, 41–66.
URL https://www.worldscientific.com/doi/abs/10.1142/S2010194511000092

Acknowledgments

Writing this thesis certainly was a memorable part in the journey of my studies. Not only did I get to meet wonderful people, but also significantly expand my knowledge. I want to thank Klaus Dolag, Rhea-Silvia Remus and Benjamin Seidel for providing me with this very interesting project, that reminded me exactly why i wanted to pursue astrophysics in the first place. With the help of Rheas motivational speeches and encouragement, even the for me least enjoyable parts of this work turned into a rather fun experience, thank you for that! I also appreciate how inspiring you are, encouraging me to stay creative and not loose sight of the real purpose of any seemingly tiring task. I also want to thank the whole DRAGONS group for welcoming me with open arms and including me in group meetings letting me get a glimpse into the whole scientific work progress. Special thanks to Anna Ivleva for sharing wise words when I needed to hear them to stay motivated.

This whole thesis would never have been possible without the endless support of Benjamin Seidel who always had time to spare for my many many questions. Regardless of how insignificant the initial question seemed to be, the partly hour long discussions that followed always yielded interesting insights. Without you it would not have been possible to gain such deep understanding in such a short time. Thank you for answering all questions even when I lost myself in ever so small details. Thank you for encouraging me to stay curious and for explaining complex concepts over and over until i really understood them.

Finally, I want to thank my friends and family for supporting me throughout this whole experience and also the various people that helped me proof read my thesis. I specially want to thank Alexandra Konrad for pointing me to Rheas group, without you I would not have stumbled across the DRAGONS group to begin with. I especially want to thank Samuel Stallybrass for always having my back, without your emotional support i would not have made it this far.

Selbstständigkeitserklärung

Hiermit erkläre ich, die vorliegende Arbeit selbstständig verfasst zu haben und keine anderen als die in der Arbeit angegebenen Quellen und Hilfsmittel benutzt zu haben.

München, 17.06.2024

Mein Name